Geosci. Model Dev. Discuss., https://doi.org/10.5194/gmd-2018-247
Manuscript under review for journal Geosci. Model Dev.
Discussion started: 7 November 2018


# FFNN-LSCE: A two-step neural network model for the reconstruction of surface ocean $pCO_2$ over the Global Ocean.

Anna Denvil-Sommer[1], Marion Gehlen[1], Mathieu Vrac[1], Carlos Mejia[2]

[1]Laboratoire des Sciences du Climat et de l'Environnement (LSCE), Institut Pierre Simon Laplace (IPSL), CNRS/CEA/UVSQ/Univ. Paris-Saclay, Orme des Merisiers, Gif-Sur-Yvette, 91191, France

[2]Sorbonne Université, CNRS, IRD, MNHN, Institut Pierre Simon Laplace (IPSL), Paris, 75005, France

*Correspondence to*: Anna Denvil-Sommer (anna.sommer.lab@gmail.com)

**Abstract.**

A new Feed-Forward Neural Network (FFNN) model is presented to reconstruct surface ocean partial pressure of carbon dioxide ($pCO_2$) over the global ocean. The model consists of two steps: (1) reconstruction of $pCO_2$ climatology and (2) reconstruction of $pCO_2$ anomalies with respect to the climatology. For the first step, a gridded climatology was used as the target, along with sea surface salinity and temperature (SSS and SST), sea surface height (SSH), chlorophyll *a* (Chl), mixed layer depth (MLD), as well as latitude and longitude as predictors. For the second step, data from the Surface Ocean $CO_2$ Atlas (SOCAT) provided the target. The same set of predictors was used during step 2 augmented by their anomalies. During each step, the FFNN model reconstructs the non-linear relations between $pCO_2$ and the ocean predictors. It provides monthly surface ocean $pCO_2$ distributions on a 1°x1° grid for the period 2001-2016. Global ocean $pCO_2$ was reconstructed with a satisfying accuracy compared to independent observational data from SOCAT. However, errors are larger in regions with poor data coverage (e.g. Indian Ocean, Southern Ocean, subpolar Pacific). The model captured the strong interannual variability of surface ocean $pCO_2$ with reasonable skills over the Equatorial Pacific associated with ENSO (El Niño Southern Oscillation). Our model was compared to three $pCO_2$ mapping methods that participated in the Surface Ocean $pCO_2$ Mapping intercomparison (SOCOM) initiative. We found a good agreement in seasonal and interannual variabilty between the models over the global ocean. However, important differences still exist at the regional scale, especially in the Southern hemisphere and in particular, the Southern Pacific and the Indian Ocean, as these regions suffer from poor data-coverage. Large regional uncertainties in reconstructed surface ocean $pCO_2$ and sea-air $CO_2$ fluxes have a strong influence on global estimates of $CO_2$ fluxes and trends.

Geosci. Model Dev. Discuss., https://doi.org/10.5194/gmd-2018-247
Manuscript under review for journal Geosci. Model Dev.
Discussion started: 7 November 2018

Geoscientific Model Development Discussions

## 1. Introduction.

The global ocean is a major sink of excess $CO_2$ emitted to the atmosphere since the beginning of the industrial revolution. In 2011, the best estimate of the ocean inventory of anthropogenic carbon ($C_{ant}$) amounted to 155 ± 30 PgC or 28% of cumulated total $CO_2$ emissions attributed the human activities since 1750 (Ciais et al., 2013). Between 2000 and 2009, the yearly average ocean $C_{ant}$ uptake was 2.3 ± 0.7 PgC $yr^{-1}$ (Ciais et al., 2013). These global estimates hide, however, substantial regional and inter-annual fluctuations (Rödenbeck et al., 2015), which need to be quantified in order to track the evolution of the Earth's carbon budget (e.g. Le Quéré et al., 2018).

Until recently, most estimates of inter-annual air-sea $CO_2$ flux variability were based on atmospheric inversions (Peylin et al., 2005, 2013; Rödenbeck et al., 2005) or global ocean circulation models (Orr et al., 2001; Aumont and Bopp, 2006; Le Quéré et al., 2010). However, models tend to underestimate the variability of air-sea $CO_2$ fluxes (Le Quéré et al., 2003), while atmospheric inversions suffer from a still sparse network of atmospheric $CO_2$ measurements (Peylin et al., 2013). These approaches are increasingly complemented by data based techniques relying on *in situ* measurements of $CO_2$ fugacity (e.g. Landschützer et al., 2016; Rödenbeck et al., 2014, 2015; Takahashi et al., 2002, 2009, Landschützer et al., 2013; Schuster et al., 2013; Nakaoka et al., 2013; Fay et al., 2014). These techniques rely on a variety of data-interpolation approaches developed to provide estimates in time and space of surface ocean $pCO_2$ (Rödenbeck et al., 2015) such as statistical interpolation, linear and non-linear regressions, or model-based regressions or tuning (Rödenbeck et al., 2014, 2015). These methods have their advantages, as well as disadvantages and are compared and discussed in Rödenbeck et al. (2015). This intercomparison did not allow identifying a single optimal technique, but rather pleaded in favour of exploiting the ensemble of methods.

Artificial neural networks (ANN) have been widely used to reconstruct surface ocean $pCO_2$ (open ocean: Lefèvre et al., 2005; Friedrich and Oschlies, 2009b; Telszewski et al., 2009; Landschützer et al., 2013; Nakaoka et al., 2013; Zeng et al. 2014; coastal region: Laruelle et al., 2017). ANN fill the spatial and temporal gaps based on calibrated non-linear statistical relationships between $pCO_2$ and its oceanic and atmospheric drivers. The existing products usually present monthly fields with a 1°x1° spatial resolution and capture a large part of temporal-spatial variability. Methods based on ANN are able to represent the large class of $pCO_2$-driver relationships, but they are sensitive to the number of data used in the training algorithm and can generate artificial variability in regions with sparse data coverage.

This study proposes an alternative implementation of a neural network applied to the reconstruction of surface ocean $pCO_2$ over the period 2001-2016. It belongs to the category of Forward Feed Neural

Geosci. Model Dev. Discuss., https://doi.org/10.5194/gmd-2018-247
Manuscript under review for journal Geosci. Model Dev.
Discussion started: 7 November 2018

Geoscientific Model Development
Open Access
Discussions

Networks (FFNN) and consists of a two-step approach: (1) the reconstruction of monthly climatologies of global surface ocean $pCO_2$ based on data from Takahashi et al. (2009), and (2) the reconstruction of monthly anomalies (with respect to the monthly climatologies) on a 1°x1° grid exploiting the Surface Ocean $CO_2$ Atlas (SOCAT) (Bakker et al., 2016). The model is easily applied to the global ocean without any boundaries between the ocean basins or regions. However, as mentioned before, it is still sensitive to the observational coverage. This limitation is partly overcome by the two-step approach as the reconstruction of monthly climatologies draws on a larger data set, thereby keeping FFNN output close to realistic values. Furthermore, the reconstruction of monthly climatologies during the first step allows taking into account a potential change in seasonal cycle in response to climate change when applied to time slices or to model output providing the drivers, but no carbon cycle variables.

The remainder of this paper is structured as follows: section 2 introduces data sets used during this study and describes the neural network; section 3 presents results for its validation and qualification, as well as a comparison to three mapping methods part of the Surface Ocean $pCO_2$ Mapping intercomparison (SOCOM) exercise (Rödenbeck et al., 2015). Results and perspectives are summarized in the last section.

## 2. Data and method.

### 2.1. Data.

The standard set of variables known to represent physical, chemical and biological drivers of surface ocean $pCO_2$ – mean state and variability – (Takahashi et al., 2009; Landschützer et al., 2013) were used as input variables (or predictors) for training the FFNN algorithm. These are sea surface salinity (SSS), sea surface temperature (SST), mixed layer depth (MLD), chlorophyll *a* concentration (CHL), atmospheric $CO_2$ mole fraction ($xCO_{2,atm}$). Based on Rodgers et al. (2009) who reported a strong correlation between natural variations in dissolved inorganic carbon (DIC) and sea surface height (SSH), SSH was added as a new driver to this list.

For the first step, the reconstruction of monthly climatologies, the Takahashi et al. (2009) monthly $pCO_2$ gridded climatology (1°x1°) was used as the target. The original climatology was constructed by an advection-based interpolation method on a 4ºx5º grid. It was interpolated on the 1°x1° SOCAT grid which is also the final output for the FFNN.

For the second step, the observational data base SOCAT v5 (Bakker et al., 2016) provided the target. We used a gridded version of this dataset that was derived by combining all SOCAT data collected within a 1ºx1º box during a specific month. SOCAT v5 represents global observations of sea surface fugacity of $CO_2$ ($fCO_2$) over the period 1970 to 2016. It includes data from moorings, ships and drifters. These data are distributed irregularly over the global ocean with 188274 gridded measurements over the Northern hemisphere and 76065 over the Southern hemisphere. In order to ensure a satisfaying spatial and temporal data coverage, we limited the reconstruction to the period 2001-2016, which represents ~77% of the data

Geosci. Model Dev. Discuss., https://doi.org/10.5194/gmd-2018-247
Manuscript under review for journal Geosci. Model Dev.
Discussion started: 7 November 2018

Geoscientific Model Development Discussions
Open Access

base (Fig. 1(a)).

The following formula is used to convert $fCO_2$ to $pCO_2$ (Körtzinger et al., 1999):

$$fCO_2 = pCO_2 \exp\left(p \frac{B + 2\delta}{RT}\right), \quad (1)$$

where $fCO_2$ and $pCO_2$ are in µatm, p is the total pressure (Pa), R=8.314 $JK^{-1}$ is the gas constant, T is the absolute temperature (K). Parameter B ($m^3mol^{-1}$) is estimated as: B = (-1636.75 + 12.0408 T – 3.27957 * $10^{-2}$ $T^2$ + 3.16528 * $10^{-5}$ $T^3$) $10^{-6}$ . The parameter δ is the cross virial coefficient ($m^3mol^{-1}$): δ = (57.7 – 0.118T) $10^{-6}$. The total pressure is from the Jena data base (6h, 5ºx5º) (http://www.bgc-jena.mpg.de/CarboScope/?ID=s).

Monthly global observed physics reprocessed products distributed through the Copernicus Marine Environment Monitoring Service (CMEMS) (0.25ºx0.25º) (http://marine.copernicus.eu/services-portfolio/access-to-products/?option=com_csw&view=details&product_id=MULTIOBS_GLO_PHY_REP_015_002) were used for SSS, SST and SSH. The GlobColour project provided monthly CHL distributions at 1ºx1º resolution (http://www.globcolour.info/products_description.html). For MLD, daily data from the "Estimating the Circulation and Climate of the Ocean" (ECCO2) project Phase II, at 0.25ºx0.25º resolution (Menemenlis et al., 2008) were used. For $xCO_2$ atmospheric, the 6h data from Jena $CO_2$ inversion s76_v4.1 on a 5ºx5º grid were selected (http://www.bgc-jena.mpg.de/CarboScope/?ID=s). Finally, an ice mask based on daily "Operational Sea Surface Temperature and Sea Ice Analysis" (OSTIA) with a gridded 0.05ºx0.05º resolution (Donlon et al., 2011) was applied.

MLD and CHL were log-transformed before their use in the FFNN algorithm because of their skewed distribution. In regions with no CHL data (high latitudes in winter) log(CHL) = 0 was applied. It does not introduce discontinuities since log(CHL) is close to zero in the adjacent region.

All data were averaged or interpolated on a 1ºx1º grid and, depending on the resolution of the data set, averaged over the month. It is worth noting that all data sets have to be normalized (i.e. centered to zero-mean and reduced to unit standard deviation) before their use in the FFNN algorithm, for example:

$$SSS_n = \frac{SSS - S\bar{S}S}{std(SSS)} .$$

Normalization ensures that all predictors fall within a comparable range and therefore avoids giving more weight to predictors with large variability ranges (Kallache et al., 2011).

As surface ocean $pCO_2$ also varies spatially, geographical positions (lat, lon) were included as predictors. In order to normalize (lat, lon) the following transformation is proposed:

$$lat_n = \sin(lat)$$

Geosci. Model Dev. Discuss., https://doi.org/10.5194/gmd-2018-247
Manuscript under review for journal Geosci. Model Dev.
Discussion started: 7 November 2018

Geoscientific Model Development Discussions

$$lon_n 1 = \sin(lon)$$

$$lon_n 2 = \cos(lon)$$

Two functions *sin* and *cos* for longitudes are used to preserve its periodical 0 to 360 degrees behavior and thus to consider the difference of positions before and after the 0º longitude. For step 2, data required for training were co-located at the SOCAT data positions that are used as target for the FFNN model. Details are provided in the next section.

2.2. Method.

a) Network configuration and evaluation protocol

In this work we use Keras, a high-level neural network Python library ("Keras: The Python Deep Learning library", Chollet, 2015; https://keras.io) to build and train the FFNN models. The identification of an optimal configuration is the first step in the FFNN model building. This includes: the choice of number and size of hidden layers (i.e., intermediate layers between input and output layers), connection type, activation functions, loss function and optimization algorithm, as well as the learning rate and other low level parameters. Based on a series of tests and their statistical results (RMS, correlation, bias) a hyperbolic tangent was chosen as an activation function for neurons in hidden layers, and a linear function for the output layer. As optimization algorithm the mini-batch gradient descent or RMSprop was used (adaptive learning rates for each weight, Chollet, 2015; Hinton et al., 2012). The number of layers and neurons depends on the problem. For totally connected layers (i.e., a neuron in a hidden layer is connected to all neurons in the precedent layer and connects all neurons in the next one), the case here, it is enough to have only one single hidden layer but two or more can help the approximation of complex functions (or complex relations between the input and the output of the problem).

The number of the FFNN layers and number of neurons depends on one side on the complexity of the problem: the more layers and neurons, the better the accuracy of output. However, the size also depends on the number of patterns (data) used for training. There is a well-known empirical rule advising to have a factor of 10 between number of patterns (data) and number of connections, or weights to adjust. This limits the size, the number of parameters and incidentally the number of neurons, of the FFNN. This empirical rule was followed in this study.

(1) Step 1: reconstruction of monthly climatologies

FFNN reconstructs a monthly surface ocean $pCO_2$ climatology as a nonlinear function of SSS, SST, SSH, Chl, MLD and geographical position (longitude, latitude):

Geosci. Model Dev. Discuss., https://doi.org/10.5194/gmd-2018-247
Manuscript under review for journal Geosci. Model Dev.
Discussion started: 7 November 2018


$$pCO_{2,n} = \left(SSS_n, SST_n, SSH_n, Chl_n, MLD_n, lon_n, lat_n\right) \quad (2)$$

Surface ocean $pCO_2$ from Takahashi et al. (2009) provided the target. The data set was divided into 50% for FFNN training and 25% for its evaluation. This 25% did not participate in the training. This set is used to monitor process performance and drive convergence. The remaining 25% (each 4th point) of the data set were used after training for the FFNN model validation. More details about the FFNN training process can be found in Rumelhart et al. (1986) and Bishop (1995). Validation and evaluation data sets were chosen quasi-regularly in space and time to take into account all regions and seasonal variability. In order to improve the accuracy of the reconstruction, the model was applied separately for each month. Tests with one model for 12 months showed a slight decrease in accuracy (not presented here). We have developed a FFNN model with 5 layers (3 hidden layers). About 17500 data were available for each month to train the model, resulting in monthly FFNN models with about 1856 parameters.

(2) Step 2: reconstruction of anomalies

During the second step, $pCO_2$ anomalies were reconstructed as a nonlinear function of SSS, SST, SSH, Chl, MLD, $xCO_2$ and their anomalies, as well as geographic position:

$$pCO_{2,n,anom} = \left(SSS_n, SST_n, SSH_n, Chl_n, MLD_n, xCO_{2,n}, SSS_{anom,n}, SST_{anom,n}, SSH_{anom,n}, Chl_{anom,n}, MLD_{anom,n}, xCO_{2,\,anom,n}, lon_n 1, lon_n 2, lat_n\right) \quad (3)$$

Surface ocean $pCO_2$ anomalies computed as the differences between collocated $pCO_2$ values based on SOCAT observations and monthly $pCO_2$ climatologies reconstructed during the first step provided the targets:

$$pCO_{2,anom} = pCO_{2,SOCAT} - pCO_{2,clim,FFNN} \quad (4)$$

The set of target data was again divided into 50% for the training algorithm, 25% for evaluation and 25% for model validation. As in step (1) the model was trained separately for each month. There were thus 12 models sharing a common architecture but trained on different data. At this step, in order to increase the amount of data during training and to introduce information on the seasonal cycle, the model was trained using as a target $pCO_2$ data from the month in question as well as those from the previous and following month during the entire period 2001-2016. Figures 1 (b) and 1 (c) show an example of data distribution for the sole months of January over the period 2001-2016 (Fig. 1 (b)) and for the three months time-window December-January-February 2001-2016 used in the training algorithm of the January FFNN model (Fig. 1 (c)). In this particular example, the choice of three months provided a better cover of the region and doubled the number of data at high latitudes.

K-fold cross-validation was used for evaluation and validation of the FFNN architecture. Cross-validation relied on K=4 different subsampling of the data set to draw 25% of independent data for validation (Fig. S1). Each sampling was tested on 5 runs of the FFNN for each month. Each of these 5 runs is characterized

Geosci. Model Dev. Discuss., https://doi.org/10.5194/gmd-2018-247
Manuscript under review for journal Geosci. Model Dev.
Discussion started: 7 November 2018

Geoscientific Model Development Discussions
Open Access EGU

by different initial values that are chosen automatically. From these 5 results, the best was chosen based on root-mean-square-error (RMSE), $r^2$ and bias.

The final model architecture had 3 layers (1 hidden layer). About 10000 samples were available for training for each month, thus, a model with 541 parameters was developed. Note that a higher number of parameters did not show a significant improvement of accuracy (not shown).

b) Reconstruction of surface ocean $pCO_2$

The previous section presented the development of a FFNN model for the reconstruction of global surface ocean $pCO_2$, and the estimation of its accuracy. It allowed to identify the "optimal" FFNN architecture for the reconstruction of surface $pCO_2$ and its validation. This FFNN model was used to provide the final product for scientific analysis and comparison with other mapping approaches. In order to provide the final output, the selected FFNN architecture is trained on all available data: 100% of data for training, 100% for evaluation and 100% for validation. The network was executed 5 times (different initial values) and the best model was selected based on validation results considering root-mean-square-error (RMSE), correlation and bias computed between network output and SOCAT derived surface ocean $pCO_2$ data. The final model output is referred to as the FFNN-LSCE product.

2.3. Computation of sea-air $CO_2$ fluxes.

Sea-air $CO_2$ flux *f* was calculated following Rödenbeck et al. (2015) as:

$$f = k\rho L\left(pCO_2 - pCO_2^{atm}\right) \qquad (5)$$

where k is the piston velocity estimated according to Wanninkhof (1992):

$$k = \Gamma u^2\left(Sc^{CO_2}/Sc^{Ref}\right)^{-0.5} \quad . \qquad (6)$$

The global scaling factor $\Gamma$ was chosen as in Rödenbeck et al. (2014) with the global mean $CO_2$ piston velocity equaling to 16.5 cm/h. *Sc* corresponds to the Schmidt number estimated according to Wanninkhof (1992). The wind speed was computed from 6-hourly NCEP wind speed (Kalnay et al., 1996). $\rho$ stands for seawater density in (4) and L for temperature-dependent solubility (Weiss, 1974). $pCO_2$ corresponds to the surface ocean $pCO_2$, output of the mapping method. $pCO_2^{atm}$ was derived from the atmospheric $CO_2$ mixing ratio fields provided by the Jena inversion (http://www.bgc-jena.mpg.de/CarboScope/).

## 3. Results.

### 3.1. Validation.

The subset of data used for network validation, that is 25% of the total, represents independent observations

Geosci. Model Dev. Discuss., https://doi.org/10.5194/gmd-2018-247
Manuscript under review for journal Geosci. Model Dev.
Discussion started: 7 November 2018

Geoscientific Model Development Discussions
Open Access
EGU

as they did not participate in training. The skill of the FFNN to reconstruct monthly climatologies of surface ocean $pCO_2$, was assessed by comparing collocated reconstructed $pCO_2$ and corresponding values from Takahashi et al. (2009). The global climatology was reconstructed with a satisfying accuracy during step 1 with a RMSE of 0.17 µatm and $r^2$ of 0.93. Model output of step 2 was assessed by K-fold cross validation as presented before: K=4 different subsamplings of independent data were drawn from the data set and the network was run 5 times on each subsampling. From these 20 results the best one was chosen based on RMSE, $r^2$ and bias. The combination of the four best model output was used for the statistical analysis summarized in Table 1. Metrics were computed over the full period (2001-2016) and with reference to SOCAT observations (independent data only). At the global scale, the analysis yielded a RMSE of ~17.97 µatm, while the absolute bias was 11.52 µatm and $r^2$ 0.76. These results are comparable to those obtained by Landschützer et al. (2013) for the assessment of a surface ocean $pCO_2$ reconstruction based on an alternative neural network based approach. The RMSE between SOCAT data and the climatology of $pCO_2$ from Takahashi et al. (2009) equals 41.87 µatm, larger than erros computed for the regional comparison between FFNN and SOCAT (Table 1).

Figure 2 (a) shows the time mean difference between the estimated $pCO_2$ and $pCO_2$ from SOCAT v5 data used for validation $mean_t\left(pCO_{2,i,j,FFNN}-pCO_{2,i,j,SOCAT}\right)$. Large differences occurred at high latitudes, in equatorial regions, along the Gulf Stream and Kuroshio currents – the regions with strong horizontal gradient of $pCO_2$. Moreover the standard deviation of residuals (Figure 2 (b)) in these regions was larger indicating that the model fails to accurately reproduce the temporal variability. The reduced skill of the model in these regions reflects the poor data coverage along with a strong seasonal variability (e.g. Southern Ocean) and/or high kinetic energy (e.g. Southern Ocean, Kuroshio and Gulf Stream currents) (Fig. 1 (a)). At the scale of ocean regions, (Table 1) the largest RMSE and bias were computed for the Pacific Subpolar ocean (RMSE = 34.77 µatm, biais = 23.12 µatm), while the lowest correlation coefficient was obtained for the equatorial Atlantic ocean ($r^2$ = 0.57). These low scores directly reflect low data density and are to be contrasted with those obtained over regions with better data coverage (e.g. Subtropical Pacific: RMSE = 15.86 µatm, biais = 9.9 µatm, $r^2$ = 0.77 or Subpolar Atlantic: RMSE = 22.99 µatm, biais = 15.04 µatm, $r^2$ = 0.76). Despite large time mean differences computed over the eastern Equatorial Pacific, scores are satisfying at the regional scale indicating error compensation by improved scores over the western basin. Scores are low in the Southern hemisphere (Table 1) and time mean differences are large (Fig. 2 (a)) reflecting sparse data coverage (Fig. 1 (a)).

### 3.2. Qualification.

This section presents the assessment of the final time series of reconstructed surface ocean $pCO_2$. The time series was computed using the best monthly models as described in section 2.2, as well as 100% of data for

Geosci. Model Dev. Discuss., https://doi.org/10.5194/gmd-2018-247
Manuscript under review for journal Geosci. Model Dev.
Discussion started: 7 November 2018

Geoscientific Model Development Discussions
Open Access

learning, evaluation and validation.

Results of the FFNN-LSCE mapping model were compared to three published mapping methods which participated in the "Surface Ocean pCO2 Mapping Intercomparison" (SOCOM) exercise presented in Rödenbeck et al. (2015) (http://www.bgc-jena.mpg.de/SOCOM/). These methods are: (1) Jena-MLS (Rödenbeck et al., 2014), a statistical interpolation scheme (data-driven mixed-layer scheme; principal drivers: ocean-internal carbon sources/sinks, SST, wind speed, mixed-layer depth climatology, alkalinity climatology); (2) JMA-MLR (Iida et al., 2015), based on multi-linear regressions with SST, SSS and Chl *a* as independent variables, and (3) ETH-SOMFFN (Landschützer et al., 2014), a combined two-step neural network model with SST, SSS, MLD, Chl *a*, $xCO_2$ as drivers. Qualification followed methods and analyses proposed by Rödenbeck et al. (2015). The time series of $pCO_2$ and sea-air flux $CO_2$ (*f*) were assessed over 17 biomes defined by Fay and McKinley (2014) (Fig. 3, Table 2). These biomes were derived based on coherence in SST, Chl *a*, ice fraction, maximum MLD and represent regions of coherent biogeochemical dynamics.

We followed the protocol and diagnostics proposed in Rödenbeck et al. (2015) for the comparison of the mapping methods between each other, respectively to observations. The following diagnostics were computed: (1) the relative interannual variability (IAV) mismatch $R^{iav}$ (in %) and (2) the amplitude of interannual variations. The relative interannual variability (IAV) mismatch $R^{iav}$ (in %) is the ratio of the mismatch amplitude $M^{iav}$ of the difference between the model output and observations (its temporal standard deviation) and the mismatch amplitude $M^{iav}_{benchmark}$ of the "benchmark". The later was derived from the mean seasonal cycle of the corresponding model output where the trend of increasing yearly atmospheric $pCO_2$ was added (see details in Rödenbeck et al., 2015). It corresponds to a climatology corrected for increasing atmospheric $CO_2$, but without interannual variability.

$$R^{iav} = \frac{M^{iav}}{M^{iav}_{benchmark}} * 100\% \quad , (6)$$

where

$$M^{iav} = std\left(mean\left(pCO_{2,Model} - pCO_{2,SOCAT}\right)\right) \, ,$$

$$M^{iav}_{benchmark} = std\left(mean\left(D_{season}\right)\right) \, ,$$

where "mean" is a mean over the region and year and

$$D_{season} = \left(pCO_{2,SS} + trend\left(CO_{2,atm}\right)\right) - pCO_{2,SOCAT} \, ,$$

$pCO_{2,SS}$ is the seasonal cycle of $pCO_2$ from the corresponding mapping method. $CO_{2,atm}$ estimates from $xCO_2$ Jena $CO_2$ inversion s76_v4.1 were used.

$R^{iav}$ provides information on the capability of each method to reproduce the IAV compared to observations: a smaller $R^{iav}$ stands for better fit compared to the reference. The amplitude of the interannual variations,

Geosci. Model Dev. Discuss., https://doi.org/10.5194/gmd-2018-247
Manuscript under review for journal Geosci. Model Dev.
Discussion started: 7 November 2018

Geoscientific Model Development
Discussions

$A^{iav}$, of sea-air flux of $CO_2$ (its 2-month running mean). $A^{iav}$ is estimated as the temporal standard deviation over the period.

3.2.1. Interannual variability.

The time series of global averaged surface ocean $pCO_2$ over the period 2001-2016 are presented in Figure 4 for FFNN-LSCE and the three other models. Surface ocean $pCO_2$ (µatm) varied between 4 mapping methods in the range of ±7 µatm (Fig. 4 (a)). Modeled $pCO_2$ values were at the lower end for ETH-SOMFFN and JMA-MLR, while FFNN-LSCE and Jena-MLS13 computed higher values. The same behavior was found for 12-month running mean time series (Fig. 4 (b)). Figure 4 (c) shows the 12-month running mean of difference between computed $pCO_2$ and SOCAT data (model – SOCAT) over the globe. JMA-MLR mostly underestimated observed $pCO_2$ with a strong interannual variability of the misfit, especially at the end of the period with up to -5 µatm. The difference between ETH-SOMFFN output and SOCAT data fluctuates in the range of ±1 µatm, with an increase in amplitude up to -2 µatm from 2010 onward. Jena-MLS13 overestimated observations with the difference in the range of 0-1 µatm. The difference between FFNN-LSCE and SOCAT varies around zero between -0.7 and 1 µatm.

The model was assessed next at biome scale. Results for all biomes are presented in the supplementary material (Fig. S2, S3, S4). Two biomes with contrasting dynamics are discussed hereafter in greater detail: (1) the Equatorial East Pacific (biome 6) characterized by a strong IAV of surface ocean $pCO_2$ and sea-air $CO_2$ fluxes in response to ENSO, the El Niño Southern Oscillation (Feely et al., 1999; Rödenbeck et al., 2015), and (2) North Atlantic Permanently Stratified biome (biome 11) with a well-marked seasonal cycle, but little IAV (Schuster et al., 2013). Results for these biomes are presented in Figure 5.

Biome 6 is relatively well-covered by observations and represents a key region for testing the skill of the model to reproduce the observed strong IAV linked to ENSO. El Niño events are characterized by positive SST anomalies, reduced upwelling and decreased surface ocean $pCO_2$ values. These episodes could be identified in all model time series (Fig. 5 (a)) with reduced $pCO_2$ levels in 2004/2005 and 2006/2007 (weak El Niño), 2002/2003 and 2009/2010 (moderate El Niño), and 2015/2016 (strong El Niño). JMA-MLR (blue curve) tended to underestimate $pCO_2$ during weak El Niño events. It was underestimated during the La Niña 2011-2012 event by Jena-MLS13. FFNN-LSCE and ETH-SOMFFN, both based on a neural network approach yielded similar results despite differences in network architecture and predictor data sets.

Data coverage is particularly high over Biome 11 (Fig. 5 (b), (d), (f)). The seasonal cycle in this biome is dominantly driven by temperature. Modeled seasonal variability showed a good agreement across the ensemble of methods (Fig. 5(b)) with an increase in spring-summer and a decrease in autumn-winter.

Geosci. Model Dev. Discuss., https://doi.org/10.5194/gmd-2018-247
Manuscript under review for journal Geosci. Model Dev.
Discussion started: 7 November 2018

Geoscientific Model Development Discussions
Open Access
EGU

However, the amplitude can be different by up to 10 µatm between different models. The seasonal amplitude of $pCO_2$ computed by JMA-MLR increased from smaller values at the beginning of the time series to higher ones in the middle of the period 2005-2012. The variability of seasonal amplitude was the highest for Jena-MLS13 in line with the 12-month running mean time series (Fig. 5 (d)). Again, similar seasonal amplitude and year-to-year variability of surface ocean $pCO_2$ were obtained with FFNN-LSCE and ETH-SOMFFN (Fig. 5 (b), (d)). The yearly $pCO_2$ mismatch (Fig. 5 (f)) shows that observed surface ocean $pCO_2$ was underestimated by JMA-MLR at the beginning and at the end of the period by up to -6 µatm, and overestimated during 2007-2011 by up to 8 µatm. Jena-MLS13 shows mostly positive differences in the range 0-2 µatm over the full period. FFNN-LSCE and ETH-SOMFFN vary around zero and between -2 – 2 µatm, being close to each other.

3.2.2. Sea-air $CO_2$ flux variability.

Sea-air exchange of $CO_2$ was estimated using the same gas exchange formulation (4) and wind data speed (6-hourly NCEP wind speed) for each mapping data (Rödenbeck et al., 2005). It is worth noting that the sea-air flux is sensitive to the choice of wind speed data set (Roobaert et al., 2018).

Figure 6 (a) presents the global 12-month running mean of the air-sea $CO_2$ flux for four mapping methods. All models showed an increase in $CO_2$ uptake in response to increasing atmospheric $CO_2$ levels, albeit with a strong between-model variability in multi-annual trends. There is less agreement between the methods compared to reconstructions of surface ocean $pCO_2$ variability (Fig. 4 (b)). This results from the contribution of uncertainties in air-sea $CO_2$ flux estimations over regions with poor data-coverage (mostly in the South Hemisphere: South Pacific, South Atlantic, Indian Ocean, South Ocean; see Fig. S5). Nevertheless, the relative IAV mismatch was less than 30% for all methods (Fig. 6 (b)), suggesting a reasonable fit to observational data. The relative IAV mismatch is, however, a global score and it is biased towards regions with good data coverage (Rödenbeck et al., 2015). The time series reconstructed in this study is too short to capture decadal variations and in particular the strengthening of the sink from 2000 onward (Landschützer et al., 2016). FFNN-LSCE computed a slowdown of ocean $CO_2$ uptake between 2010 and 2013 with a flux of ~-1.8 GtC $yr^{-1}$ compared to ~-2.2 GtC $yr^{-1}$ for ETH-SOMFFN. A leveling-off was also found for JMA-MLR, albeit shifted in time. In general, the amplitudes of reconstructed $CO_2$ fluxes across all four methods agreed within 0.2-0.36 PgC/yr. The weighted mean of IAV (horizontal line in Fig. 6 (b)) computed from the four methods included here was 0.253 PgC/yr. This value is close to the one of Rödenbeck et al. (2015) for the complete ensemble of SOCOM models (0.31 PgC/yr) estimated for the period 1992-2009. The largest amplitude was obtained for ETH-SOMFFN, ~0.348 PgC/yr. On the other hand, FFNN-LSCE has the smallest amplitude with 0.206 PgC/yr. Jena-MLS13 and JMA-MLR lie very close to the weighted mean value with 0.257 PgC/yr and 0.221 PgC/yr, respectively. The weighted mean and the dispersion of individual models around it, reflect the period of analysis (2001-2015, ETH-SOMFFN output provided up to 2015) and the total number of models contributing to it (see for comparison Rödenbeck et al., 2015). As such it does not provide information on the skill of any particular model.

The interannual variability of reconstructed sea-air $CO_2$ fluxes (12-month running mean) showed a good agreement for biome 6 (East Pacific Equatorial, Fig. 7 (a)). A small discrepancy was found at the beginning of the period. A strong increase was computed by Jena-MLS13 for 2010-2014 that was also identified on $pCO_2$ variability (Fig. 5 (a)). Despite this Jena-MLS13 has a low relative IAV (26.24%). This confirms a tendency mentioned in Rödenbeck et al. (2015) that mapping products with a small IAV show larger amplitude. FFNN-LSCE and ETH-SOMFFN yielded comparable results (Fig. 7 (a), (c)) with relative IAV mismatches of 46.13% and 53.26%, respectively, and with amplitudes ~ 0.03 PgC/yr. Interannual variability reproduced by JMA-MLR falls within the range of the other models (Fig. 7 (c)), but with a $R^{IAV}$ of ~68.46%.

Reconstructed sea-air $CO_2$ fluxes over the North Atlantic Subtropical Permanently Stratified region (biome 11) show large between model differences in amplitudes and variability. The two models based on a neural network show again a good agreement with $R^{IAV}$ of 17% for FFNN-LSCE and 20% for ETH-SOMFFN. Jena-MLS13 produced a strong seasonal variability (Fig. 7 (b)) up to 0.06 PgC/yr, and small $R^{IAV}$ of ~11%. JMA-MLR did not reproduce a decrease of sea-air $CO_2$ at the middle of period by up to 0.02 PgC/yr (Fig. 7 (b)). The model is characterized by a $R^{IAV}$ of 46.48% and an amplitude of 0.013 PgC/yr.

### 3.3.3. Sea-air $CO_2$ flux trend.

The long-term trend of sea-air $CO_2$ fluxes is dominantly driven by the increase in atmospheric $CO_2$ (see Fig. S7). On shorter time scales, such as for the period 2001-2016, the interannual variability at regional scale reflects natural mode of climate variability and local oceanographic dynamics (Heinze et al., 2015).

Figure 8 shows the linear trends of sea-air $CO_2$ fluxes for FFNN-LSCE (a), Jena-MLS13 (b), ETH-SOMFFN (c) and JMA-MLR (d). A total negative trend was computed for all models, albeit with large regional contrasts, and FFNN-LSCE fallen within the range: Jena-MLS13, -0.0028 PgC/yr; FFNN-LSCE, -0.0032 PgC/yr; JMA-MLR, -0.0037 PgC/yr; ETH-SOMFFN, -0.0059 PgC/yr. FFNN-LSCE computed negative trends over most of the Atlantic basin, Indian Ocean and South of 40°S, which contrasts with decreasing fluxes over the Pacific and locally in the Antarctic Circumpolar current. At first order this broad regional pattern is found in all models. Regional maxima and minima are, however, more pronounced in Jena-MLS13 (Fig. 8 (b)) and ETH-SOMFFN (Fig. 8 (c)), while a patchy distribution at sub-basin scale is

Geosci. Model Dev. Discuss., https://doi.org/10.5194/gmd-2018-247
Manuscript under review for journal Geosci. Model Dev.
Discussion started: 7 November 2018


Geoscientific Model Development Discussions
Open Access

diagnosed for JMA-MLR.

The agreement in sign of computed linear trends from four models is presented in Fig. 9. Over most of the ocean, all four models show very close sea-air $CO_2$ tendency. In the Indian Ocean (biome 14), on the other hand a positive trend was computed for JMA-MLR (0.0004 PgC/yr) while the three other models present a negative trend. These differences between models were also found in the Pacific Ocean, especially the Southern Pacific. In the Eastern Equatorial Pacific region (biome 6) a total negative trend equal to $-4.03 \times 10^{-5}$ PgC/yr was computed for ETH-SOMFFN, which contrasts with positive trends suggested by FFNN-LSCE ($6.68 * 10^{-5}$ Pg/C/yr) and Jena-MLS13 ($3 * 10^{-4}$ PgC/yr). All models reproduced a maximum in the southern part of biome 6 but they disagree about its amplitude and spatial distribution. Almost everywhere over the Atlantic Ocean the mapping methods produced the same sign of linear trend (Fig. 9). Only in the eastern part of the subtropical North Atlantic Jena-MLS13 gave a positive linear trend of $fCO_2$ (Fig. 8 (b)).

According to FFNN-LSCE, the global ocean took up in average 1.55 PgC/yr between 2001-2015.This estimate is consistent with results from the other three models (Table 3) (see Table S1 for estimations per biomes). The spread between individual models falls in the range of the error reported in Landschützer et al. (2016), ±0.4-0.6 PgC/yr. Per biome, estimates of $CO_2$ sea-air fluxes provided by FFNN-LSCE are similarly in good agreement with those derived from the other models.

## 4. Summary and conclusion.

We proposed a new model for the reconstruction of monthly surface ocean $pCO_2$. The model is applied globally and allows a seamless reconstruction without introducing boundaries between the ocean basins or bioms. Our model relies on a two-step approach based on Feed-Forward Neural Networks (FFNN-LSCE). The first step corresponds to the reconstruction of a monthly $pCO_2$ climatology. It allows us to keep the output of the FFNN close to the observed values in the region with the poor data cover. Moreover, it allows to include a potential change in seasonal cycle in response to climate change from drivers to carbon cycle variables. At the second step $pCO_2$ anomalies are reconstructed according to climatology from the first step. The model was applied over the period 2001-2016. Validation with independent data at global scale indicated an accuracy of 17.57 µatm, $r^2$ of ~0.76 and an absolute bias of 11.52 µatm. In order to assess the model further, it was compared to three different mapping models: ETH-SOMFFN (self-organizing maps + neural network), Jena-MLS13 (statistical interpolation), JMA-MLR (linear regression) (Rödenbeck et al., 2015). Network qualification followed the protocol and diagnostics proposed in Rödenbeck et al. (2015). Reconstructed surface ocean $pCO_2$ distributions were in good agreement with other models and observations. The seasonal variability was reproduced satisfyingly by FFNN-LSCE, the yearly $pCO_2$

mismatch varied around zero, and relative IAV mismatch was 7.55%. FFNN-LSCE proved skillful in reproducing the interannual variability of surface ocean $pCO_2$ over the Eastern Equatorial Pacific in response to ENSO. Reductions in surface ocean $pCO_2$ during El Niño events were well reproduced. The comparison between reconstructed and observed $pCO_2$ values yielded a RMSE of 15.73 µatm, $r^2$ of 0.79 and an absolute bias of 10.33 µatm over the Equatorial Pacific. The relative IAV misfit in this region was ~17%. Despite an overall good agreement between models, important differences still exists at the regional scale, especially in the Southern hemisphere and in particular, the Southern Pacific and the Indian Ocean. These regions suffer from poor data-coverage. Large regional uncertainties in reconstructed surface ocean $pCO_2$ and sea-air $CO_2$ fluxes have a strong influence on global estimates of $CO_2$ fluxes and trends.

**Code and data availability.**

Python code for $pCO_2$ climatology reconstruction, 1st step of FFNN-LSCE model:
https://files.lsce.ipsl.fr/public.php?service=files&t=016351132f69db55f1e6eda948665237

Python code for reconstruction of $pCO_2$ anomalies, 2nd step of FFNN-LSCE model:
https://files.lsce.ipsl.fr/public.php?service=files&t=9304199cf79efd688837e891383287c3

Data of FFNN-LSCE $pCO_2$ are available on request: anna.sommer.lab@gmail.com

**Author contribution.**

ADS, MG, MV and CM contributed to the development of the methodology and designed the experiments, ADS carried them out. ADS developed the model code and performed the simulations. ADS prepared the manuscript with contributions from all co-authors.

**Acknowledgments.**

Authors would like to thank Frederic Chevallier and Gilles Reverdin for their suggestions. Authors would like to gratefully acknowledge funding by the AtlantOS project (EU Horizon 2020 research and innovation program, grant agreement no. 2014-633211). MV also acknowledges funding by the CoCliServ project (ERA4CS program).

**References**

Aumont, O., and Bopp, L.: Globalizing results from ocean in situ iron fertilization studies, Global Biogeochem. Cycles, 20, GB2017, doi:10.1029/2005GB002591, 2006.

Bakker, D. C. E., Pfeil, B., Landa, C. S., Metzl, N., O'Brien, K. M., Olsen, A., Smith, K., Cosca, C., Harasawa, S., Jones, S. D., Nakaoka, S.-I. et al.: A multi-decade record of high-quality f$CO_2$ data in version 3 of the Surface Ocean $CO_2$ Atlas (SOCAT), Earth Syst. Sci. Data, 8, 383–413, https://doi.org/10.5194/essd-8-383-2016, 2016.

Bishop, C.M.: Neural Networks for Pattern Recognition, Oxford Univ. Press, Cambridge, U. K., 1995.

Bricaud, A., Mejia, C., Blondeau-Patissier, D., Claustre, H., Crepon, M., and Thiria, S.: Retrieval of pigment concentrations and size structure of algal populations from the absorption spectra using multilayered perceptrons, Appl. Opt., 46, 8, 1251-1260, 2006.

Chollet, F., et al.: Keras. https://keras.io, 2015.

Ciais P., Sabine C., Bala G. et al.: Carbon and other biogeochemical cycles. In: Climate Change 2013: The Physical Science Basis. Contribution of Working Group I to the Fifth Assessment Report of the Intergovernmental Panel on Climate Change[Stocker, T. F., D. Qin, G.-K. Plattner, M. Tignor, S. K. Allen, J. Boschung, A. Nauels, Y. Xia, V. Bex and P. M. Midgley (eds.)]. Cambridge University Press, Cambridge, United Kingdom and New York, NY, USA, 2013.

Donlon, C.J., Martin, M., Stark, J.D., Roberts-Jones, J., Fiedler, E., and Wimmer, W.: The Operational Sea Surface Temperature and Sea Ice analysis (OSTIA), Remote Sensing of the Environment, doi: 10.1016/j.rse.2010.10.017, 2011.

Fay, A. R. and McKinley, G. A.: Global open-ocean biomes: mean and temporal variability, Earth Syst. Sci. Data, 6, 273–284, doi:10.5194/essd-6-273-2014, 2014.

Fay, A.R., McKinley, G.A., and Lovenduski, N.S.: Southern Ocean carbon trends: Sensitivity to methods, Geophys. Res. Lett., 41, 6833–6840, doi:10.1002/2014GL061324, 2014.

Feely, R. A., Wanninkhof, R., Takahashi, T., and Tans, P.: Influence of El Niño on the equatorial Pacific contribution to atmospheric $CO_2$ accumulation, Nature, 398, 597–601, 1999.

Friedrich, T., and Oschlies, A.: Basin-scale p$CO_2$ maps estimated from ARGO float data: A model study, J. Geophys. Res., 114, C10012, doi:10.1029/2009JC005322, 2009a.

Friedrich, T., and Oschlies, A.: Neural network-based estimates of North Atlantic surface p$CO_2$ from satellite data: A methodological study, J. Geophys. Res., 114, C03020, doi: 10.1029/2007JC004646, 2009b.

Gross, L., Thiria, S., Frouin, R., and Mitchell, B.G.: Artificial neural networks for modeling transfer function between marine reflectance and phytoplankton pigment concentration, J. Geophys. Res., 105, C2, 3483-3949, doi: 10.1029/1999jc900278, 2000.

Hinton, G., Srivastava, N., and Swersky, K.: Lecture 6a: Overview of mini-batch gradient descent. Neural Networks for Machine Learning. Slides: http://www.cs.toronto.edu/~tijmen/csc321/slides/lecture_slides_lec6.pdf, 2012.

Iida, Y., Kojima, A., Takatani, Y., Nakano, T., Midorikawa, T., and Ishii, M.: Trends in p$CO_2$ and sea-air $CO_2$ flux over the global open oceans for the last two decades, J. Oceanogr., 71, 637–661, doi:10.1007/s10872-015-0306-4, 2015.

Kalnay, E., Kanamitsu, M., Kistler, R., Collins, W., Deaven, D., Gandin, L., Iredell, M., Saha, S., White, G., Woollen, J., Zhu, Y., Chelliah, M., Ebisuzaki, W., Higgins, W., Janowiak, J., Mo, K. C., Ropelewski, C.,

Geosci. Model Dev. Discuss., https://doi.org/10.5194/gmd-2018-247
Manuscript under review for journal Geosci. Model Dev.
Discussion started: 7 November 2018


Geoscientific Model Development Discussions
Open Access

Wang, J., Leetmaa, A., Reynolds, R., Jenne, R., and Joseph, D.: The NCEP/NCAR 40-year reanalysis project, B. Am. Meteorol. Soc., 77, 437–471, 1996.

Kallache, M., Vrac, M., Naveau, P., Michelangeli, P.-A.: Non-stationary probabilistic downscaling of extreme precipitation, J. Geophys. Res. - Atmospheres, 116, D05113, doi:10.1029/2010JD014892, 2011.

Körtzinger, A.: Methods of Seawater Analysis, chap. Determination of carbon dioxide partial pressure ($pCO_2$), 149–158, Verlag Chemie, 1999.

Landschützer, P., Gruber, N., Bakker, D. C. E., Schuster, U., Nakaoka, S., Payne, M. R., Sasse, T. P., and Zeng, J.: A neural network-based estimate of the seasonal to inter-annual variability of the Atlantic Ocean carbon sink, Biogeosciences, 10, 7793–7815, https://doi.org/10.5194/bg-10-7793-2013, 2013.

Landschützer, P., Gruber, N., Bakker, D. C. E., and Schuster, U.: Recent variability of the global ocean carbon sink, Global Biogeochem. Cy., 28, 927–949, https://doi.org/10.1002/2014GB004853, 2014.

Landschützer, P., Gruber, N. & Bakker, D. C. E.: Decadal variations and trends of the global ocean carbon sink, Glob. Biogeochem. Cycles, 30, 1396–1417, https://doi.org/10.1002/2015GB005359, 2016.

Laruelle, G. G., Landschützer, P., Gruber, N., Tison, J.-L., Delille, B., and Regnier, P.: Global high-resolution monthly $pCO_2$ climatology for the coastal ocean derived from neural network interpolation, Biogeosciences, 14, 4545-4561, https://doi.org/10.5194/bg-14-4545-2017, 2017.

Lefèvre, N., Watson, A. J., and Watson, A. R.: A comparison of multiple regression and neural network techniques for mapping *in situ* $pCO_2$ data, Tellus, 57B, 375–384, https://doi.org/10.3402/tellusb.v57i5.16565, 2005.

Le Quéré, C., and Coauthors: Two decades of ocean $CO_2$ sink and variability, Tellus, 55B, 649–656, https://doi.org/10.1034/j.1600-0889.2003.00043.x, 2003.

Le Quéré, C., Takahashi, T., Buitenhuis, E. T., Rödenbeck, C., and Sutherland, S. C.: Impact of climate change and variability on the global oceanic sink of $CO_2$, Glob. Biogeochem. Cy., 24, GB4007, doi:10.1029/2009GB003599, 2010.

Le Quéré, C., Andrew, R. M., Friedlingstein, P., Sitch, S., Pongratz, J., Manning, A. C., et al.: Global carbon budget 2017, Earth System Science Data, 10 (1), 405–448. https://doi.org/10.5194/essd-10-405-2018, 2018.

Majkut, J. D., Carter, B.R., Frölicher, T.L., Dufour, C.O., Rodgers, K.B., and Sarmiento, J.L.: An observing system simulation for Southern Ocean carbon dioxide uptake, Philos. Trans. Roy. Soc. London, A372, 20130046, doi:https://doi.org/10.1098/rsta.2013.0046, 2014.

Mejia, C., Thiria, S., Tran, N., and Crepon, M.: Determination of the Geophysical Model Function of ERS1 Scatterometeer by the use of Neural Networks, J. Geophys. Res., Vol. 103, No. C6, PP 12853-12868, https://doi.org/10.1029/97JC02178, 1998.

Menemenlis, D., Campin, J., Heimbach, P., Hill, C., Lee, T., Nguyen, A., Schodlok, M., and Zhang, H.: ECCO2: High resolution global ocean and sea ice data synthesis, Mercator Ocean, Quarterly Newsletter, 31, 13–21, 2008.

Nakaoka, S., Telszewski, M., Nojiri, Y., Yasunaka, S., Miyazaki, C., Mukai, H., and Usui, N.: Estimating temporal and spatial variation of ocean surface pCO2 in the North Pacific using a self-organizing map neural network technique, Biogeosciences, 10, 6093–6106, doi:10.5194/bg-10-6093-2013, 2013.

Geosci. Model Dev. Discuss., https://doi.org/10.5194/gmd-2018-247
Manuscript under review for journal Geosci. Model Dev.
Discussion started: 7 November 2018


Geoscientific Model Development Discussions
Open Access

Organelli, E., Barbieux, M., Claustre, H., Schmechtig, C., Poteau, A., Bricaud, A., Boss, E., Briggs, N., Dall'Olmo, G., D'Ortenzio, F., Leymarie, E., Mangin, A., Obolensky, G., Penkerc'h, C., Prieur, L., Roesler, C., Serra, R., Uitz, J., and Xing, X.: Two databases derived from BGC-Argo float measurements for marine biogeochemical and bio-optical applications, Earth Syst. Sci. Data, 9, 861-880, https://doi.org/10.5194/essd-9-861-2017, 2017.

Orr, J. C., Monfray, P., Maier-Reimer, E., Mikolajewicz, U., Palmer, J., Taylor, N. K., Toggweiler, J. R., Sarmiento, J. L., Quere, C. L., Gruber, N., Sabine, C. L., Key, R. M. and Boutin, J.: Estimates of anthropogenic carbon uptake from four three-dimensional global ocean models, Global Biogeochem. Cycl., 15, 43–60, https://doi.org/10.1029/2000GB001273, 2001.

Peylin, P., Bousquet, P., Le Quéré, C., Sitch, S., Friedlingstein, P., McKinley, G., Gruber, N., Rayner, P., and Ciais, P.: Multiple constraints on regional $CO_2$ flux variations over land and oceans, Glob. Biogeochem. Cycles, 19, GB1011, https://doi.org/10.1029/2003GB002214, 2005.

Peylin, P., Law, R. M., Gurney, K. R., Chevallier, F., Jacobson, A. R., Maki, T., Niwa, Y., Patra, P. K., Peters, W., Rayner, P. J., Rödenbeck, C., van der Laan-Luijkx, I. T., and Zhang, X.: Global atmospheric carbon budget: results from an ensemble of atmospheric $CO_2$ inversions, Biogeosciences, 10, 6699-6720, https://doi.org/10.5194/bg-10-6699-2013, 2013.

Rödenbeck, C.: Estimating $CO_2$ sources and sinks from atmospheric mixing ratio measurements using a global inversion of atmospheric transport, Technical Report 6, Max Planck Institute for Biogeochemistry, Jena, available at: http://www.bgc-jena.mpg.de/uploads/Publications/TechnicalReports/tech_report6.pdf, 2005.

Rödenbeck, C., Bakker, D. C. E., Metzl, N., Olsen, A., Sabine, C., Cassar, N., Reum, F., Keeling, R. F., and Heimann, M.: Interannual sea-air $CO_2$ flux variability from an observation-driven ocean mixed-layer scheme, Biogeosciences, 11, 4599–4613, doi:10.5194/bg-11-4599-2014, 2014.

Rödenbeck, C., Bakker, D. C. E., Gruber, N., Iida, Y., Jacobson, A. R., Jones, S., Landschützer, P. et al.: Data-based estimates of the ocean carbon sink variability—first results of the Surface Ocean $pCO_2$ Mapping intercomparison (SOCOM), Biogeosciences, 12, 7251–7278, https://doi.org/10.5194/bg-12-7251-2015, 2015.

Rodgers, K. B., Key, R. M., Gnanadesikan, A., Sarmiento, J. L., Aumont, O., Bopp, L. et al.: Using altimetry to help explain patchy changes in hydrographic carbon measurements, J. Geophys. Res., 114, C09013, doi:10.1029/2008JC005183, 2009.

Roobaert, A., Laruelle, G. G., Landschützer, P., and Regnier, P.: Uncertainty in the global oceanic CO2 uptake induced by wind forcing: quantification and spatial analysis, Biogeosciences, 15, 1701-1720, https://doi.org/10.5194/bg-15-1701-2018, 2018.

Rumelhart, D.E., Hinton, G.E., & Williams, R.J.: Learning internal representations by backpropagating errors, Nature, 323, 533–536, 1986.

Sauzède, R., Claustre, H., Uitz, J., Jamet, C., Dall'Olmo, G., D'Ortenzio, F., Gentili, B., Poteau, A., and Schmechtig, C.: A neural network-based method for merging ocean color and Argo data to extend surface bio-optical properties to depth: Retrieval of the particulate backscattering coefficient, J. Geophys. Res. Oceans, 121, 2552–2571, doi:10.1002/2015JC011408, 2016.

Schuster, U., McKinley, G. A., Bates, N., Chevallier, F., Doney, S. C., Fay, A. R., González-Dávila, M., Gruber, N., Jones, S., Krijnen, J., Landschützer, P., Lefèvre, N., Manizza, M., Mathis, J., Metzl, N., Olsen,

Geosci. Model Dev. Discuss., https://doi.org/10.5194/gmd-2018-247
Manuscript under review for journal Geosci. Model Dev.
Discussion started: 7 November 2018


Geoscientific Model Development Discussions
Open Access

A., Rios, A. F., Rödenbeck, C., Santana-Casiano, J. M., Takahashi, T., Wanninkhof, R., and Watson, A. J.: An assessment of the Atlantic and Arctic sea–air CO2 fluxes, 1990–2009, Biogeosciences, 10, 607-627, https://doi.org/10.5194/bg-10-607-2013, 2013.

Takahashi, T., Sutherland, S.C., Wanninkhof, R., Sweeney, C., Feely, R.A., Chipman, D.W., Hales, B., Friederich, G., Chavez, F., Sabine, C., et al.: Climatological mean and decadal change in surface ocean $pCO_2$, and net sea-air $CO_2$ flux over the global oceans, Deep.-Sea Res. II, 56(8–10), 554–577, https://doi.org/10.1016/j.dsr2.2008.12.009, 2009.

Takahashi, T., Sutherland, S. C., Sweeney, C., Poisson, A., Metzl, N. et al.: Global sea-air $CO_2$ flux based on climatological surface ocean $pCO_2$, and seasonal biological and temperature effects, Deep.-Sea Res. II, 49, 1601–1622, https://doi.org/10.1016/S0967-0645(02)00003-6, 2002.

Telszewski, M., Chazottes, A., Schuster, U., Watson, A. J., Moulin, C., Bakker, D. C. E., González-Dávila, M., Johannessen, T., Körtzinger, A., Lüger, H., Olsen, A., Omar, A., Padin, X. A., Ríos, A. F., Steinhoff, T., Santana-Casiano, M., Wallace, D.W.R., and Wanninkhof, R.: Estimating the monthly $pCO_2$ distribution in the North Atlantic using a self-organizing neural network, Biogeosciences, 6, 1405–1421, doi:10.5194/bg-6-1405-2009, 2009.

Wanninkhof, R.: Relationship between wind speed and gas exchange over the ocean, J. Geophys. Res.-Oceans, 97, 7373–7382, https://doi.org/10.1029/92JC00188, 1992.

Weiss, R.: Carbon dioxide in water and seawater: the solubility of a non-ideal gas, Mar. Chem., 2, 203–205, https://doi.org/10.1016/0304-4203(74)90015-2, 1974.

Williams, N.L., Juranek, L.W., Feely, R.A., Johnson, K.S., Sarmiento, J.L., Talley, L.D., Dickson, A.G., Gray, A.R., Wanninkhof, R., Russell, J.L., Riser, S.C., Takeshita, Y.: Calculating surface ocean $pCO_2$ from biogeochemical Argo floats equipped with pH: An uncertainty analysis, Global Biogeochemical Cycles, 31:591-604, https://doi.org/10.1002/2016GB005541, 2017.

Zeng, J., Nojiri, Y., Landschützer, P., Telszewski, M., and Nakaoka, S.: A global surface ocean $fCO_2$ climatology based on a feed-forward neural network, J. Atmos. Ocean Technol., 31, 1838–1849, https://doi.org/10.1175/JTECH-D-13-00137.1, 2014.

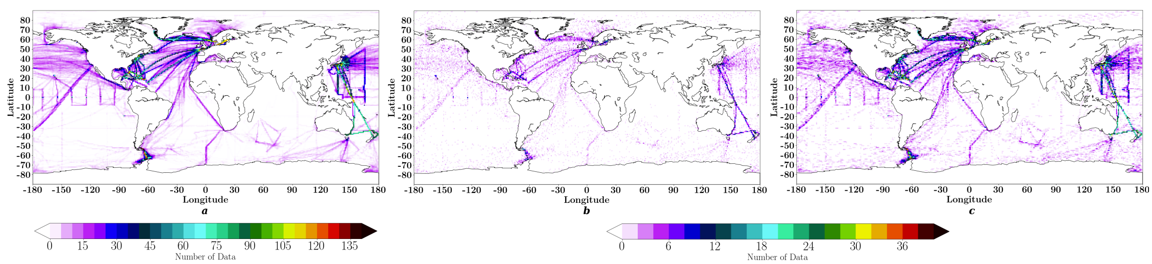


**Figure 1: Spatial distribution of SOCAT data (number of measurements per grid point): (a) - period 2001-2016; (b) - all months January for period 2001-2016; (c) - all months December-January-February for period 2001-2016.**

Geosci. Model Dev. Discuss., https://doi.org/10.5194/gmd-2018-247
Manuscript under review for journal Geosci. Model Dev.
Discussion started: 7 November 2018


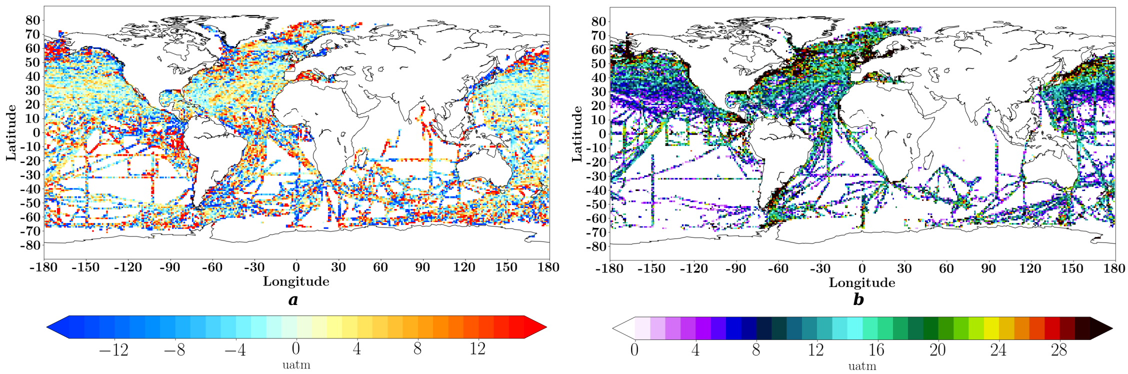


**Figure 2: Time mean differences (µatm) (a) between monthly FFNN-LSCE $pCO_2$ and SOCAT $pCO_2$ data used for evaluation of the model over the period 2001-2016 and its std (b).**

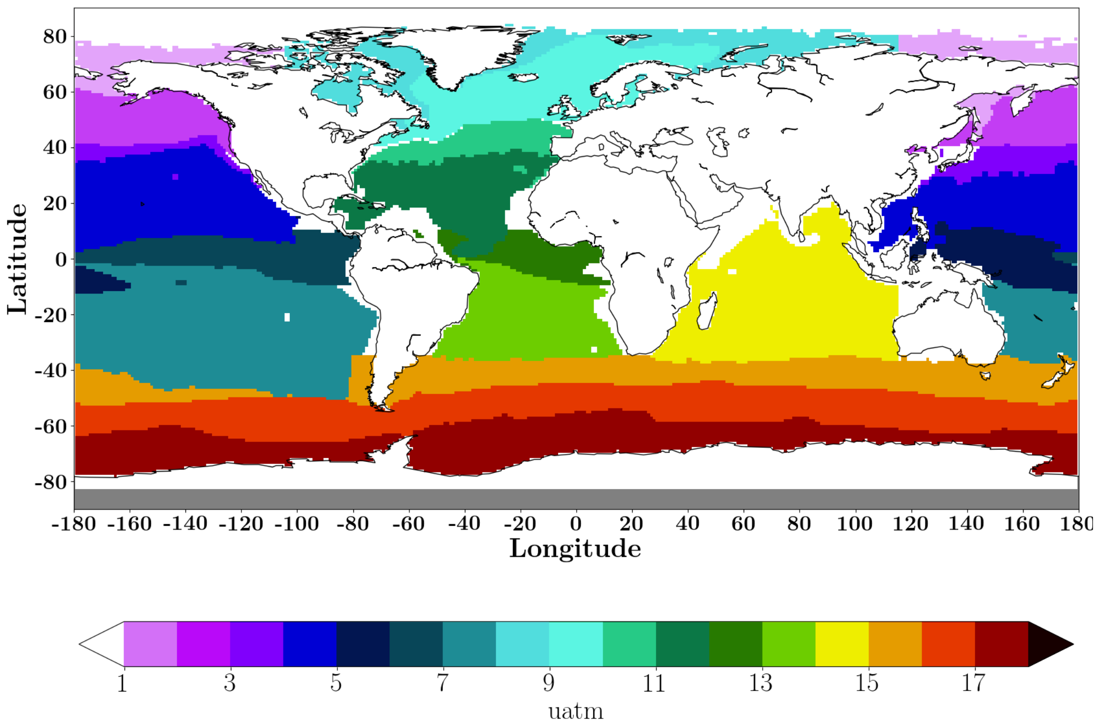


**Figure 3: Map of biomes (after Rodenbeck et al. (2015); and Fay and McKinley (2014)) used for comparison. See table 2 for biome names.**

Geosci. Model Dev. Discuss., https://doi.org/10.5194/gmd-2018-247
Manuscript under review for journal Geosci. Model Dev.
Discussion started: 7 November 2018


Geoscientific Model Development
Open Access
Discussions

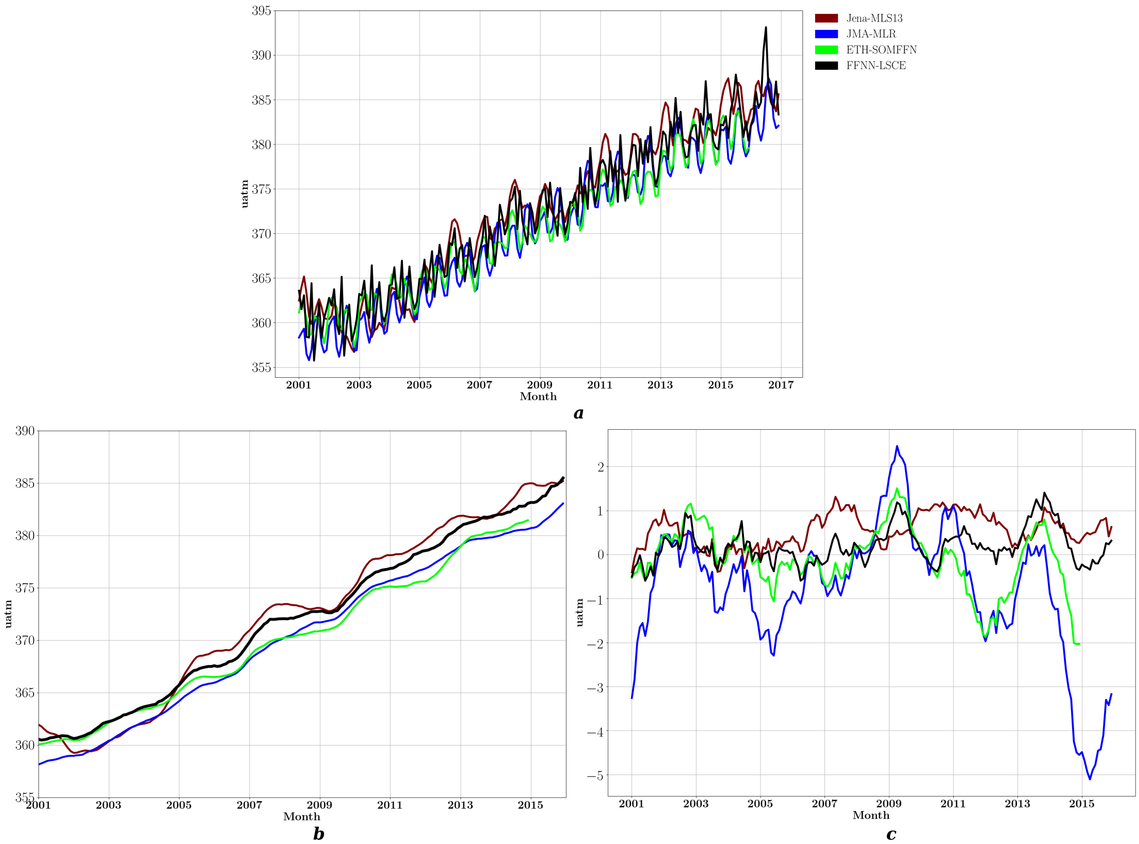


**Figure 4: Global oceanic $pCO_2$: black - FFNN-LSCE, blue - JMA, brown - Jena, green - ETH-SOMFFN; (a) - monthly time series averaged over the glob, (b) - 12-month running mean averaged over the glob, (c) - yearly $pCO_2$ mismatch (difference of mapping methods and SOCAT data).**

Geosci. Model Dev. Discuss., https://doi.org/10.5194/gmd-2018-247
Manuscript under review for journal Geosci. Model Dev.
Discussion started: 7 November 2018


Geoscientific Model Development
Discussions
Open Access

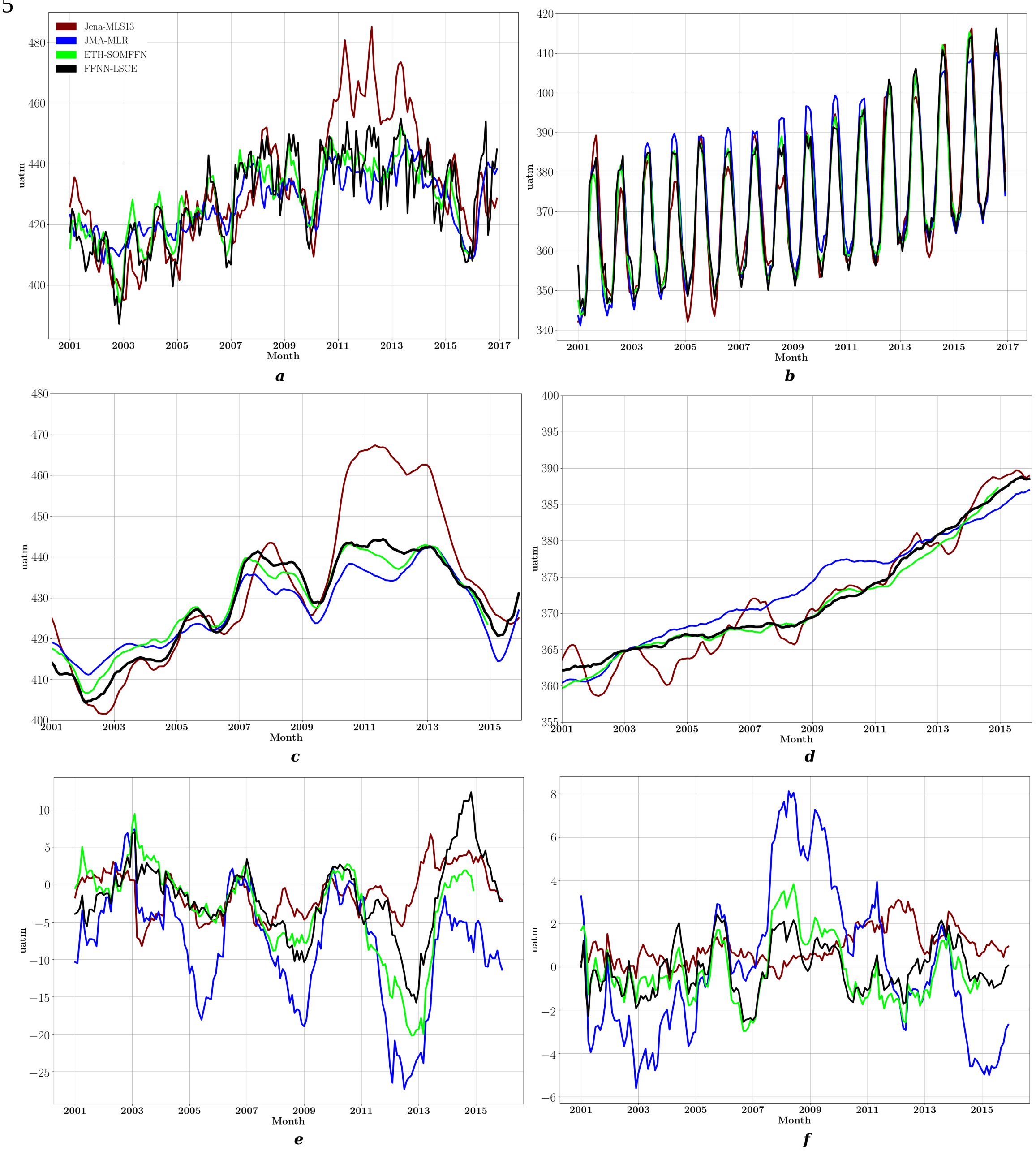


**Figure 5: East Pacific Equatorial (biome 6) (left) and North Atlantic Subtropical Permanently Stratified (biome 11) (right) oceanic $pCO_2$: black – FFNN, blue – JMA, brown – Jena, green – ETH-SOMFFN; (a), (b) – monthly time series averaged over biome; (c), (d) – 12-month running mean averaged over biome; (e), (f) – yearly $pCO_2$ mismatch (difference of mapping methods and SOCAT data).**

Geosci. Model Dev. Discuss., https://doi.org/10.5194/gmd-2018-247
Manuscript under review for journal Geosci. Model Dev.
Discussion started: 7 November 2018


Geoscientific Model Development Discussions
Open Access

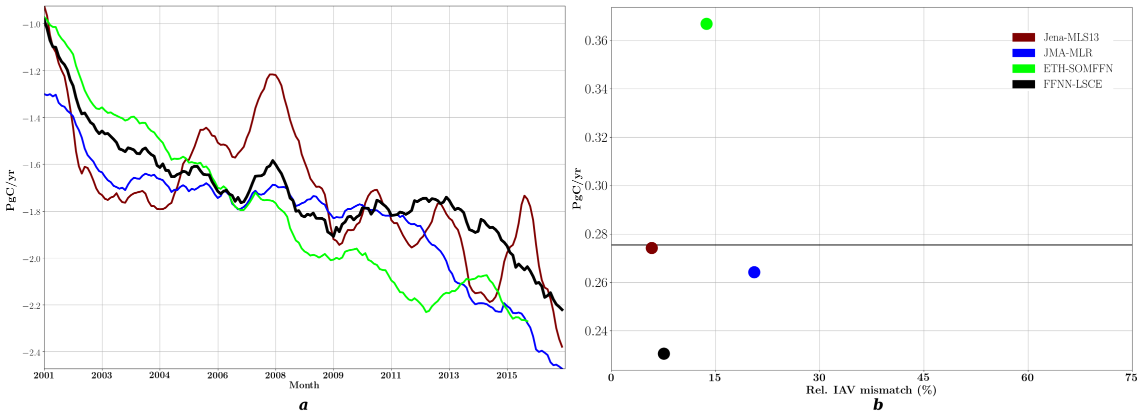


**Figure 6: (a) – Interannual sea-air $CO_2$ flux (12-month running mean) in the global ocean; (b) – amplitude of interannual $CO_2$ flux plotted against the relative IAV mismatch amplitude. The weighted mean is given as a horizontal line.**

Geosci. Model Dev. Discuss., https://doi.org/10.5194/gmd-2018-247
Manuscript under review for journal Geosci. Model Dev.
Discussion started: 7 November 2018


Geoscientific Model Development
Discussions
Open Access

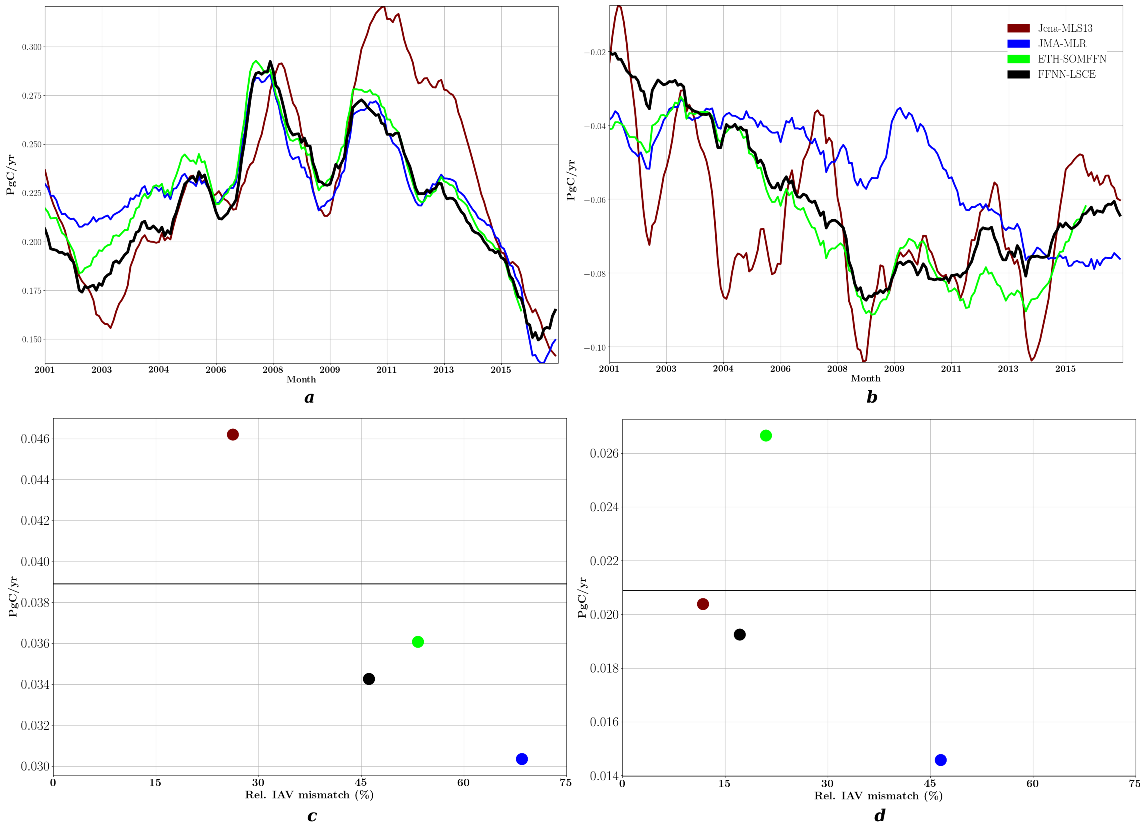


**Figure 7: East Pacific Equatorial (biome 6) (left) and North Atlantic Subtropical Permanently Stratified (biome 11) (right): (a), (b) – Interannual sea-air $CO_2$ flux (12-month running mean) in the global ocean; (c), (d) – amplitude of interannual $CO_2$ flux plotted against the relative IAV mismatch amplitude. The weighted mean is given as a horizontal line.**

Geosci. Model Dev. Discuss., https://doi.org/10.5194/gmd-2018-247
Manuscript under review for journal Geosci. Model Dev.
Discussion started: 7 November 2018


Geoscientific Model Development Discussions Open Access

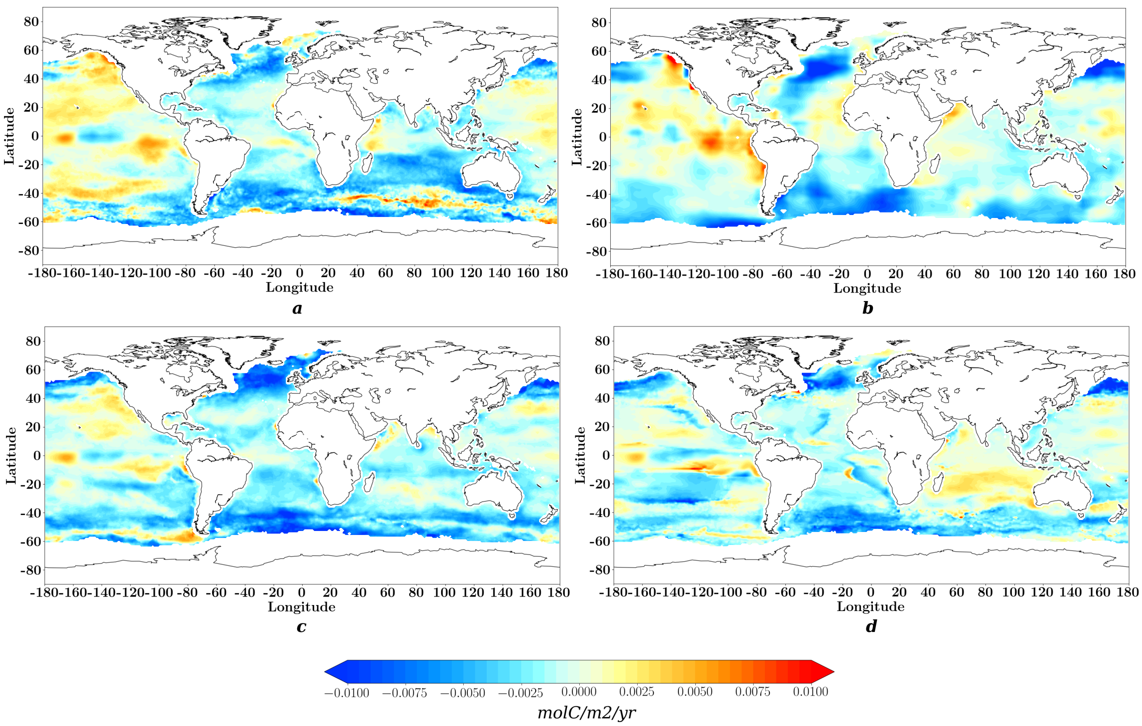


**Figure 8: Linear trend of $fCO_2$ for common period 2001-2015: (a) – FFNN-LSCE; (b) – Jena-MLS13; (c) – ETH-SOMFFN; (d) – JMA-MLR.**

702

Geosci. Model Dev. Discuss., https://doi.org/10.5194/gmd-2018-247
Manuscript under review for journal Geosci. Model Dev.
Discussion started: 7 November 2018

Geoscientific Model Development Discussions
Open Access

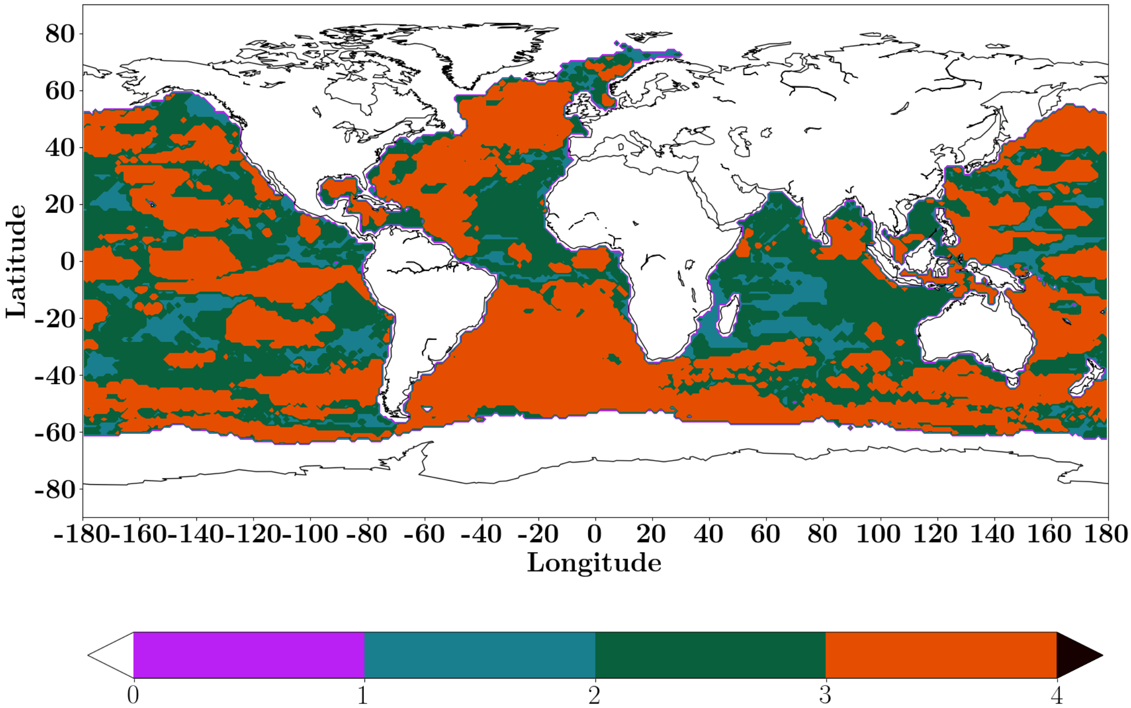


**Figure 9: Agreement between four mapping methods in their linear trend of sea-air $CO_2$ flux. Color-bar represents the number of products that have the same sign of linear trend.**

Table 1: Statistical validation of FFNN-LSCE. Comparison between reconstructed surface ocean $pCO_2$ and $pCO_2$ values from SOCAT v5 data base not used in the training algorithm for the period 2001-2016 over the global ocean (except for regions with ice-cover) and for large oceanographic regions. In round brackets:

number of measurements per region

| Model | Latitude boundaries | RMS (µatm) | $r^2$ | Bias (µatm) |
|---|---|---|---|---|
| FFNN Global | | 17.97 | 0.76 | 11.52 |
| Arctic (150) | 76ºN to 90ºN | 22.05 | 0.54 | 17.1 |
| Atlantic Subpolar (21903) | 49ºN to 76ºN | 22.99 | 0.76 | 15.04 |
| Pacific Subpolar (4529) | 49ºN to 76ºN | 34.77 | 0.65 | 23.12 |
| Atlantic Subtropical (41331) | 18ºN to 49ºN | 17.28 | 0.69 | 11.27 |
| Pacific Subtropical (41867) | 18ºN to 49ºN | 15.86 | 0.77 | 9.9 |
| Atlantic Equatorial (7300) | 18ºS to 18ºN | 17.27 | 0.57 | 11.44 |
| Pacific Equatorial (27092) | 18ºS to 18ºN | 15.73 | 0.79 | 10.33 |
| South Atlantic (3002) | 44ºS to 18ºS | 17.81 | 0.63 | 12.28 |
| South Pacific (12934) | 44ºS to 18ºS | 13.52 | 0.63 | 9.36 |
| Indian Ocean (2871) | 44S to 30N | 17.25 | 0.62 | 11.6 |
| Southern Ocean (16334) | 90ºS to 44ºS | 17.4 | 0.58 | 11.92 |

Table 2: Biomes from Fay and McKinley (2014) used for time series comparison (Fig. 3)

| Number | Name |
|---|---|
| 1 | (Omitted) North Pacific Ice |
| 2 | North Pacific Subpolar Seasonally Stratified |
| 3 | North Pacific Subtropical Seasonally Stratified |
| 4 | North Pacific Subtropical Permanently Stratified |
| 5 | West Pacific Equatorial |
| 6 | East Pacific Equatorial |
| 7 | South Pacific Subtropical Permanently Stratified |
| 8 | (Omitted) North Atlantic Ice |
| 9 | North Atlantic Subpolar Seasonally Stratified |
| 10 | North Atlantic Subtropical Seasonally Stratified |
| 11 | North Atlantic Subtropical Permanently Stratified |
| 12 | Atlantic Equatorial |
| 13 | South Atlantic Subtropical Permanently Stratified |
| 14 | Indian Ocean Subtropical Permanently Stratified |

Geosci. Model Dev. Discuss., https://doi.org/10.5194/gmd-2018-247
Manuscript under review for journal Geosci. Model Dev.
Discussion started: 7 November 2018

Geoscientific Model Development Discussions
Open Access
EGU

| | |
|---|---|
| 15 | Southern Ocean Subtropical Seasonally Stratified |
| 16 | Southern Ocean Subpolar Seasonally Stratified |
| 17 | Southern Ocean Ice |

Table 3: Mean of sea-air $CO_2$ flux (PgC/yr) over the Global Ocean and per regions for period in common (2001-2015). Averages over the period 2001-2009 are presented between brackets. The last column presents a comparison to best estimates from Schuster et al. (2013) for the Atlantic Ocean (1990 – 2009).

| Region | Latitude boundaries | FFNN-LSCE | ETH-SOMFFN | Jena-MLS13 | JMA-MLR | Schuster et al. (2013), 1990-2009 |
|---|---|---|---|---|---|---|
| Global | | -1.55 (-1.44) | -1.67 (-1.47) | -1.55 (-1.41) | -1.74 (-1.62) | --- |
| Arctic | 76ºN to 90ºN | -0.001 | -0.001 | -0.001 | -0.001 | -0.12±0.06 |
| Atlantic Subpolar | 49ºN to 76ºN | -0.15 (-0.15) | -0.14 (-0.12) | -0.15 (-0.15) | -0.16 (-0.15) | -0.21±0.06 |
| Pacific Subpolar | 49ºN to 76ºN | -0.003 (-0.005) | -0.009 (-0.004) | -0.006 (-0.004) | -0.027 (-0.021) | --- |
| Atlantic Subtropical | 18ºN to 49ºN | -0.21 (-0.19) | -0.21 (-0.19) | -0.2 (-0.18) | -0.21 (-0.2) | -0.26±0.06 |
| Pacific Subtropical | 18ºN to 49ºN | -0.45 (-0.46) | -0.49 (-0.48) | -0.47 (-0.46) | -0.49 (-0.47) | --- |
| Atlantic Equatorial | 18ºS to 18ºN | 0.085 (0.09) | 0.085 (0.095) | 0.08 (0.082) | 0.1 (0.11) | 0.12±0.04 |
| Pacific Equatorial | 18ºS to 18ºN | 0.42 (0.41) | 0.4 (0.4) | 0.44 (0.42) | 0.38 (0.37) | --- |
| South Atlantic | 44ºS to 18ºS | -0.17 (-0.16) | -0.18 (-0.16) | -0.18 (-0.17) | -0.23 (-0.22) | -0.14±0.04 |
| South Pacific | 44ºS to 18ºS | -0.33 (-0.34) | -0.4 (-0.39) | -0.35 (-0.34) | -0.49 (-0.47) | --- |
| Indian Ocean | 44S to 30N | -0.25 (-0.2) | -0.32 (-0.29) | -0.27 (-0.26) | -0.27 (-0.29) | --- |
| South Ocean | 90ºS to 44ºS | -0.38 | -0.29 | -0.36 | -0.26 | --- |